

Simulation of the Postexposure Bake Process of Chemically Amplified Resists by Reaction–Diffusion Equations

Tsung-Lung Li

Department of Applied Physics, National Chia-Yi University, 300 Hsueh-Fu Road, Chiayi 600, Taiwan

E-mail: quantum@cspl.phys.ncyu.edu.tw

Received January 10, 2001; revised July 6, 2001

In this work, a time-dependent postexposure bake (PEB) simulator is presented by solving a set of reaction–diffusion equations modeling the deprotection reaction of polymers and the diffusion of acids in chemically amplified resists. The simulator is time-dependent in the sense that model parameters including both reaction parameters and diffusion coefficients are treated as time-dependent functions in the entire course of the PEB process. The alternating direction implicit method is utilized to iteratively solve the set of reaction–diffusion equations. An error-control scheme is devised for automatic time-stepping. This PEB simulator is, hence, capable of simulating the effects of the temperature–time history of a wafer. It is then applied to simulate the resist profiles of line/space patterns and contact holes. © 2001 Academic Press

Key Words: postexposure bake; chemically amplified resists; DUV lithography; reaction–diffusion equations; alternating direction implicit; PEB simulators.

1. INTRODUCTION

Lithography in the deep submicrometer era employs photoresists whose working principles are very different from those of previous generations [1]. Photoacids are generated as the chemically amplified resist (CAR) is exposed to deep ultraviolet (DUV) radiation. The resist film with the latent image of photoacids is then baked at elevated temperature. In this postexposure bake (PEB) process, the inhibitors of the resist undergo a catalytic reaction with the photoacids and are gradually annihilated for the case of positive CARs. At the end of the PEB process, the resist in the exposed area is thus deprotected and has a much larger development rate than in the unexposed area.

The PEB process of CARs includes the reaction of inhibitors and photoacids as well as the diffusion of photoacids [2]. To physically model the process, it is necessary to couple the two mechanisms. It appears from the literature that there are three categories of PEB

models. First, the diffusionless models ignore the diffusion phenomena and consider only the reaction mechanism [3–6]. Second, the reaction–diffusion models involve both reaction and diffusion mechanisms [7–11]. Third, the moving boundary transport models include the volatility of deprotection by-products and the relaxation of free volume [12, 13]. Among the three PEB models, the moving boundary transport model is the most general and complicated one. The reaction–diffusion model and the diffusionless model may be considered special cases of the moving boundary transport model [12].

In this article, the reaction–diffusion models are extended to include model parameters which are time-dependent during the entire course of the PEB process with the intention of simulating the heating and cooling stages of the baking process. The PEB model is then solved numerically using the alternating-direction implicit method in which the two-dimensional problem is decomposed into many one-dimensional subproblems associated with each of the two directions. An error-control scheme is developed for automatic time-stepping of the numerical scheme. This simulator is applied to simulate the resist profiles of line/space patterns and contact holes with a given temperature–time history of the wafer. The PEB processes with square-wave and exponential temperature–time history are simulated and compared.

2. POSTEXPOSURE BAKE MODELS

2.1. Physical Models

The four main constituents of chemically amplified resists are photoacid generators (PAG), inhibitors, resins, and solvents. Since the resists are applied on the wafer by spin coating, ample amounts of solvents are usually added to the resists to improve the uniformity of resist thickness across the wafer [14–17]. The solvents evaporate during the spin coating process and in the subsequent softbake process [18, 19]. The evaporation rate at the resist top surface is usually faster than at other parts of the films. The resists shrink slightly due to the solvent evaporation. Therefore, the PAG and the inhibitor concentrations are not uniform in the resists; in general, they are functions of spatial vector \vec{x} before the PEB process starts.

In the simulation of the PEB process, the PAGs and the inhibitors play major roles. The chemistry of the PEB process of the chemically amplified resists can be simplified by reaction equations which involve only the PAGs, the inhibitors, the photoacids, and the by-products,



and



where M and H are the inhibitors and the photoacids, respectively, and X and Y are the by-products of the two reactions. Reactions (1) and (2) represent the exposure and the PEB processes, respectively.

At the exposure of the DUV light, PAGs are decomposed into photoacids (H) and by-products (X). In the PEB process, the photoacids (H) react with the inhibitors (M) and produce secondary acids (H) and by-products (Y). The secondary acids, in turn, react with other reaction sites of the inhibitors as they diffuse to the proper locations. The reaction of

the photoacids with the inhibitors deprotects the resist resins. Lithographic patterns may be obtained if the resist films are subsequently developed by base-developing solution.

Thus, modeling of the PEB process should involve both the catalyzed reaction and the diffusion phenomena. The PEB process is modeled by the set of reaction–diffusion equations [7, 20]

$$\frac{\partial M}{\partial t} = -k_D M^p H^q \quad (3)$$

$$\frac{\partial H}{\partial t} = \nabla \cdot (D_H \nabla H) + \mathcal{L}_a, \quad (4)$$

with the acid-loss term being

$$\mathcal{L}_a = -k_a H^m, \quad (5)$$

where M and H are the concentration of the reactive sites of the inhibitors called the protection sites and the concentration of acids, respectively. During the PEB process, both the protection site and the acid concentrations are functions of spatial vectors, \vec{x} , and time, t . Namely, $M = M(\vec{x}, t)$ and $H = H(\vec{x}, t)$. The meanings of the rest of the symbols in the above two equations are explained in the following paragraphs.

Equation (3) models the reaction of the acids with the protection sites and is termed the reaction equation in this article. The reaction is characterized by the reaction parameter k_D and the reaction orders p and q associated with the protection sites and the acids, respectively. The deprotection reaction parameter is modeled by the Arrhenius-type relation [20]

$$k_D = k_D(T) = A_D \exp\left(-\frac{E_D}{kT}\right), \quad (6)$$

where A_D and E_D are, respectively, the preexponential constant and the activation energy of the deprotection reaction, k is the Boltzmann constant, and T is the temperature whose model will be given by the end of this section.

The diffusion equation (4) includes a regular diffusion term and a loss term (\mathcal{L}_a) on the right-hand side.

The first term on the right-hand side of Eq. (4) models the mechanical diffusion of the acids in the resist. The diffusion coefficient, D_H , depends on both the temperature and the protection-site concentration and is expressed as the product of a temperature-dependent part and a concentration-dependent part [21, 22].

$$D_H = D_H(M, M_0, T) = D_0 \exp\left(\frac{\alpha\eta}{1 + \beta\eta}\right) \quad (7)$$

with

$$\eta = \frac{M_0 - M}{M_0} \quad (8)$$

and

$$D_0 = D_0(T) = A_0 \exp\left(-\frac{E_0}{kT}\right), \quad (9)$$

where M_0 is the initial concentration of the protection sites, and η is the conversion of the inhibitors. The concentration dependence of the diffusion coefficient is modeled by the Fujita–Doolittle equation (7). The Fujita–Doolittle model is based on the free volume arguments of polymers [23, 24] and predicts the diffusion coefficient increasing with the conversion of the inhibitor, η . The parameters α and β of the model are determined by experiments to provide the quantitative dependence of the diffusion coefficient on the inhibitor conversion and are termed the α - and β -parameters in this article, respectively. A_0 and E_0 are the preexponential constant and the activation energy of the temperature-dependent part of the diffusion coefficient, respectively.

The acids generated in the catalyzed reaction need to diffuse to the appropriate locations to react with protection sites. But, in the diffusion process, the acids can be trapped in the resin. The trapped acids no longer have the chance to react with any protection sites and are considered to be lost from the modeling point of view. The second term on the right-hand side of Eq. (4) accounts for the acid loss mechanism which is modeled as a reaction with the reaction parameter k_a and the reaction order m [20]. The temperature dependence of the reaction parameters of the acid loss mechanism is given by [20]

$$k_a = k_a(T) = A_a \exp\left(-\frac{E_a}{kT}\right), \quad (10)$$

where A_a and E_a are, respectively, the preexponential constant and the activation energy of the acid loss mechanism.

To solve the reaction–diffusion equations in Eqs. (3) and (4), the initial conditions of the protection-site concentration (M), and the initial and boundary conditions of the acid concentration (H), need to be specified. These conditions will be the topics of the next two sections.

2.2. Initial Conditions

During the soft bake process, the solvent evaporates faster on the resist surface than in the bulk. Hence, the concentrations of PAGs and the protection sites, in principle, are not uniform and are denoted by $G_0(\vec{x})$ and $M_0(\vec{x})$, respectively.

During the exposure process, the inhibitors are not reactive. Thus, the initial condition of the protection-site concentration is

$$M(\vec{x}, 0) = M_0(\vec{x}). \quad (11)$$

However, the PAGs are decomposed into photoacids at the exposure of a DUV beam. Thus, for the PEB simulation, the initial condition of the acid concentration is the postexposure concentration of photoacids. If the decoupled Dill's model is used to model the exposure process, the initial condition of the acid concentration is given by [25, 26]

$$H(\vec{x}, 0) = H_0(\vec{x}) = G_0(\vec{x})[1 - e^{-CI(\vec{x})t_{\text{exp}}}], \quad (12)$$

where C and t_{exp} are the PAG decomposition rate and the exposure time, respectively, and $I(\vec{x})$ is the light intensity which follows from the exposure simulations of a given photomask pattern.

2.3. Boundary Conditions

The acid molecules are usually nonvolatile during the PEB process. Hence, the acid fluxes normal to the top and bottom resist surfaces vanish, and

$$F_s^n(t, \vec{x}) = -(D_H \nabla H) \cdot \hat{n}_s = 0, \quad (13)$$

for \vec{x} on the s th resist surface, where $F_s^n(\vec{x})$ and \hat{n}_s are, respectively, the outward normal flux of the acids and the outward unit vector normal to the s th surface, where s stands for the top or the bottom resist surface.

Because the thickness of the resist film is usually on the order of a micrometer, the resist-film dimension along the substrate surface is effectively infinite. Two boundaries at the right- and left-hand sides of the simulation domain are artificially imposed to facilitate the simulation. Vanishing acid flux conditions are utilized as the boundary conditions at the right- and left-hand sides of the simulation domain. By using these conditions, it is implicitly assumed that all physical quantities are symmetric about the two artificial boundaries of the simulation domain.

2.4. Temperature Models

The reaction parameters in Eqs. (6) and (10), and the diffusion coefficient in Eq. (9), are all temperature-dependent. If the heating and cooling phases of the PEB process are to be modeled, the temperature–time history has to be taken into account. The temperature ramping of the bake hot plate reportedly behaves according to exponential-like functions of time [19, 27]. Hence, the temperature–time history is modeled as

$$\begin{aligned} T = T(t) &= \Delta T (1 - e^{-t/\tau_h}) + T_0 & \text{if } 0 \leq t \leq t_b, \\ &= \Delta T' e^{-(t-t_b)/\tau_c} + T_0 & \text{if } t_b < t \leq t_f, \end{aligned} \quad (14)$$

with

$$\Delta T = T_f - T_0 \quad (15)$$

and

$$\Delta T' = T_f' - T_0, \quad (16)$$

where T_0 and T_f are the room and bake temperatures, respectively, τ_h and τ_c are the heating and the cooling time constants of the bake process, respectively, and the bake time is denoted by t_b . The total thermal time, t_f , includes the bake time (t_b) and the time required to chill the wafer to room temperature. In this temperature model, the total thermal time is taken so that the temperature at t_f is within 5% of $\Delta T = T_f - T_0$ from T_0 . A typical temperature–time history plot is illustrated in Fig. 1. To ensure the continuity of temperature at t_b , T_f' is given by

$$T_f' = \Delta T (1 - e^{-t_b/\tau_h}) + T_0. \quad (17)$$

3. NUMERICAL METHODS

3.1. Formulation

For a substrate without topography, the solution domain is a regular shape. Rectangular meshes of equal size are used to discretize the domain. The alternating direction implicit (ADI) method is applied to solve the reaction–diffusion equations (3) and (4) in two dimensions. In each time step, an implicit scheme is used for the protection sites; the time step is split into two half steps for the photoacids: The first half involves an implicit scheme for acids in the row direction; the second half is in the column direction. The ADI finite-difference representations of the reaction–diffusion equations are given by [28–30]

$$M_{i,j}^{n+1} = M_{i,j}^n - \Delta t \cdot k_D^{n+\frac{1}{2}} \left[\frac{1}{2} (M_{i,j}^n + M_{i,j}^{n+1}) \right]^p \left[\frac{1}{2} (H_{i,j}^n + H_{i,j}^{n+1}) \right]^q \quad (18)$$

for the reaction equation

$$\begin{aligned} & -\beta_x \left(D_{i-1,j}^{n+\frac{1}{2}} + D_{i,j}^{n+\frac{1}{2}} \right) H_{i-1,j}^{n+\frac{1}{2}} + \left[1 + \beta_x \left(D_{i-1,j}^{n+\frac{1}{2}} + 2D_{i,j}^{n+\frac{1}{2}} + D_{i+1,j}^{n+\frac{1}{2}} \right) \right] H_{i,j}^{n+\frac{1}{2}} \\ & - \beta_x \left(D_{i,j}^{n+\frac{1}{2}} + D_{i+1,j}^{n+\frac{1}{2}} \right) H_{i+1,j}^{n+\frac{1}{2}} = \beta_y (D_{i,j-1}^n + D_{i,j}^n) H_{i,j-1}^n \\ & + \left[1 - \beta_y (D_{i,j-1}^n + 2D_{i,j}^n + D_{i,j+1}^n) \right] H_{i,j}^n + \beta_y (D_{i,j}^n + D_{i,j+1}^n) H_{i,j+1}^n + \mathcal{L}_{ij}^n \end{aligned} \quad (19)$$

for the first half of a time step of diffusion, and

$$\begin{aligned} & -\beta_y (D_{i,j-1}^{n+1} + D_{i,j}^{n+1}) H_{i,j-1}^{n+1} + \left[1 + \beta_y (D_{i,j-1}^{n+1} + 2D_{i,j}^{n+1} + D_{i,j+1}^{n+1}) \right] H_{i,j}^{n+1} \\ & - \beta_y (D_{i,j}^{n+1} + D_{i,j+1}^{n+1}) H_{i,j+1}^{n+1} = \beta_x \left(D_{i-1,j}^{n+\frac{1}{2}} + D_{i,j}^{n+\frac{1}{2}} \right) H_{i-1,j}^{n+\frac{1}{2}} \\ & + \left[1 - \beta_x \left(D_{i-1,j}^{n+\frac{1}{2}} + 2D_{i,j}^{n+\frac{1}{2}} + D_{i+1,j}^{n+\frac{1}{2}} \right) \right] H_{i,j}^{n+\frac{1}{2}} + \beta_x \left(D_{i,j}^{n+\frac{1}{2}} + D_{i+1,j}^{n+\frac{1}{2}} \right) H_{i+1,j}^{n+\frac{1}{2}} + \mathcal{L}_{ij}^{n+\frac{1}{2}} \end{aligned} \quad (20)$$

for the second half of the time step of diffusion, where

$$\mathcal{L}_{ij}^n = -\delta_t k_a^n (H_{i,j}^n)^m \quad (21)$$

and

$$\delta_t = \frac{\Delta t}{2}, \quad \beta_x = \frac{\Delta t}{4(\Delta x)^2}, \quad \beta_y = \frac{\Delta t}{4(\Delta y)^2}. \quad (22)$$

Here Δx and Δy are the grid sizes in the x - and the y -directions, respectively, and $\Delta t = t_{n+1} - t_n$ is the time-step size. The subscripts including i and j and the superscripts including n are the indices of the spatial grids and the temporal steps, respectively. The reaction parameters k_a and k_D and the diffusion coefficient D (a short-hand notation for D_H) all have superscripts involving n in finite-difference equations (18) to (20) because these constants and coefficients are time-dependent. Note that $D_{i,j}^n \equiv D(M_{i,j}^n, M_{i,j}^0, T^n)$, and that the powers p , q , and m in Eqs. (18) to (20) are the reaction orders, not to be confused with the time-step index denoted by the superscript n .

3.2. Time-Stepping

A time-stepping algorithm is indispensable for a time-dependent problem such as the reaction–diffusion system of interest. The time step, Δt , is determined by requiring that the relative errors averaged over all nodal points be less than ε , namely by the error-control condition

$$\frac{1}{MN} \sum_{i=1}^M \sum_{j=1}^N \frac{1}{2} \left[\frac{|\Delta M_{ij}|}{\max(M_{ij}, R)} + \frac{|\Delta H_{ij}|}{\max(H_{ij}, R)} \right] < \varepsilon, \quad (23)$$

where ΔM_{ij} and ΔH_{ij} are, respectively, the estimated errors of the protection site and the acid concentrations at a certain time step. Here ε and R are the relative and absolute errors, respectively. The summations are over all nodal points.

3.3. Algorithm

The iterative algorithm utilizing (18) to (20) to solve the reaction–diffusion equations (3) and (4) is given as follows.

ALGORITHM 1.

1. **Compute** initial conditions: $M_{i,j}^{n=0}$ by Eq. (11), and $H_{i,j}^{n=0}$ by Eq. (12).
2. **Determine** time step, Δt , by Eq. (23).
3. **Repeat**
4. **Compute** $M_{i,j}^{n+1}$ by Eq. (18).
5. **Compute** $H_{i,j}^{n+\frac{1}{2}}$ by Eq. (19).
6. **Compute** $H_{i,j}^{n+1}$ by Eq. (20).
7. **Until convergent**
8. **Increment** n , go to 2 if not end of bake process.

Equation (18) shows that step 4 for the protection sites is an implicit scheme. Equations (19) and (20) illustrate that steps 5 and 6 for the photoacids are also implicit.

The implicit schemes in steps 5 and 6 become tridiagonal matrices as the terms in Eqs. (19) and (20) are properly assembled into matrix forms. If the boundary conditions are approximated by forward or backward finite difference, the tridiagonal matrices are symmetric. However, if the boundary conditions are represented by a higher order approximation such as the central difference, the tridiagonal matrices are nonsymmetric. The latter approach is utilized in this work.

The concentration of the protection sites is computed before the photoacids so that it may be used in the diffusion coefficients of Eqs. (19) and (20) for the computation of the photoacid concentration. These procedures are repeated until the convergence occurs. The convergence condition requires that the difference of the concentrations between two iterations be less than the relative error, ε .

The ADI scheme stated above can be easily extended to three dimensions [28–30].

4. RESULTS AND DISCUSSIONS

The two test structures that are simulated in this section are the periodical line/space (LS) and the contact hole (CH) patterns.

4.1. Simulation Parameters

As suggested by Eqs. (11) and (12), the PEB simulation model presented in this work needs to take the initial concentrations of the protection sites and the PAGs, and the light intensity distribution, as inputs to the model.

In this section, it is assumed that spin-coating does not introduce nonuniformity of the protection-site and PAG concentrations. In other words, the initial concentrations of the protection sites and the PAGs in Eqs. (11) and (12) are taken to be constants.

An exposure simulation has to be performed to attain the light intensity distribution in the resist film before the PEB simulation may be carried out. Although many exposure models are available to simulate the partially coherent radiation propagating in the resist film [31–34], the simulation of the exposure process itself is outside the scope of this article. Hence, in this work, a simple model of a plane-wave with a wavelength of 193 nm propagating in a dissipative medium is utilized [35–36].

All of the resist parameters employed in the simulation are either quoted or estimated from the literature [7, 20–22], and are summarized in Table I.

4.2. Postexposure Bake Simulations

The postexposure bake simulations of the LS and CH patterns subject to the bake temperature–time history given in Fig. 1 are presented in this section as examples of PEB simulation results. The temperature model parameters employed in Fig. 1 are the room temperature $T_0 = 23^\circ\text{C}$, the bake temperature $T_f = 100^\circ\text{C}$, the heating time constant $\tau_h = 2$ s, the cooling time constant $\tau_c = 10\tau_h$, the bake time $t_b = 60$ s, and the total thermal time $t_f = 120$ s. The resist thickness is taken to be $0.6 \mu\text{m}$ for both patterns.

The LS pattern is a periodical mask pattern with a line/space dimension of $0.15/0.25 \mu\text{m}$ and is utilized to exemplify the line-definition technology of $0.15\text{-}\mu\text{m}$ lithography. The exposure dosage ($I(\vec{x})t_{\text{exp}}$) and the initial acid concentration of the LS pattern are given in Figs. 2a and 2b in units of mJ/cm^2 and $1 \times 10^6/\mu\text{m}^3$, respectively. The heavy line segment

TABLE I
Resist Parameters

Parameters	Description	Value	Unit
M_0	Initial M concentration	50	$10^6/\mu\text{m}^3$
G_0	Initial PAG concentration	45	$10^6/\mu\text{m}^3$
p	Reaction order of M	1	None
q	Reaction order of H	1	None
m	Reaction order of acid loss	2	None
C	PAG decomposition rate	0.014	cm^2/mJ
t_{exp}	Exposure time	300	msec
A_D	Preexponential constant of deprotection reaction	1.2786×10^{12}	$\mu\text{m}^3/\text{s}$
E_D	Activation energy of deprotection reaction	1.4717	eV
A_a	Preexponential constant of acid-loss reaction	29.225	$\mu\text{m}^3/\text{s}$
E_a	Activation energy of acid-loss reaction	0.7255	eV
A_0	Preexponential constant of diffusion coefficient	8.2×10^9	$\mu\text{m}^2/\text{s}$
E_0	Activation energy of diffusion coefficient	1.099	eV
α	α -parameter of diffusion coefficient	0.5107	None
β	β -parameter of diffusion coefficient	1.0412	None

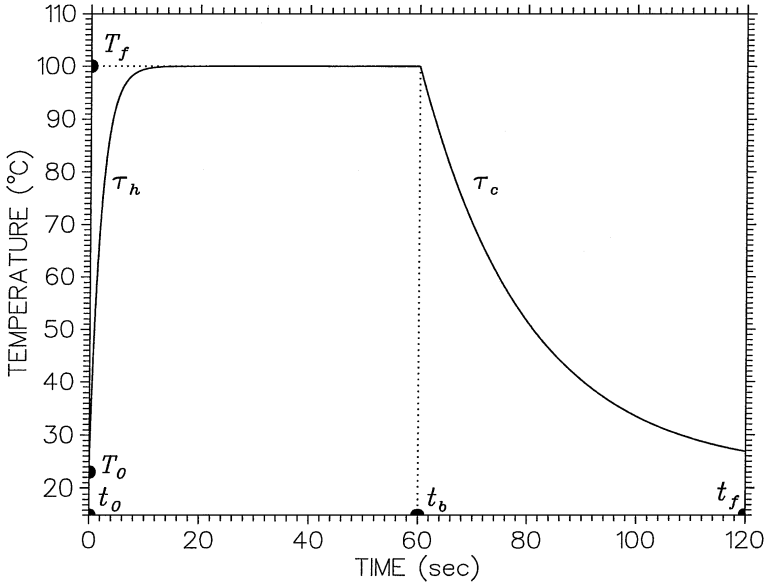


FIG. 1. An example of the temperature-time history of the PEB process is shown. The solid and dotted lines represent the exponential and square-wave PEB processes, respectively.

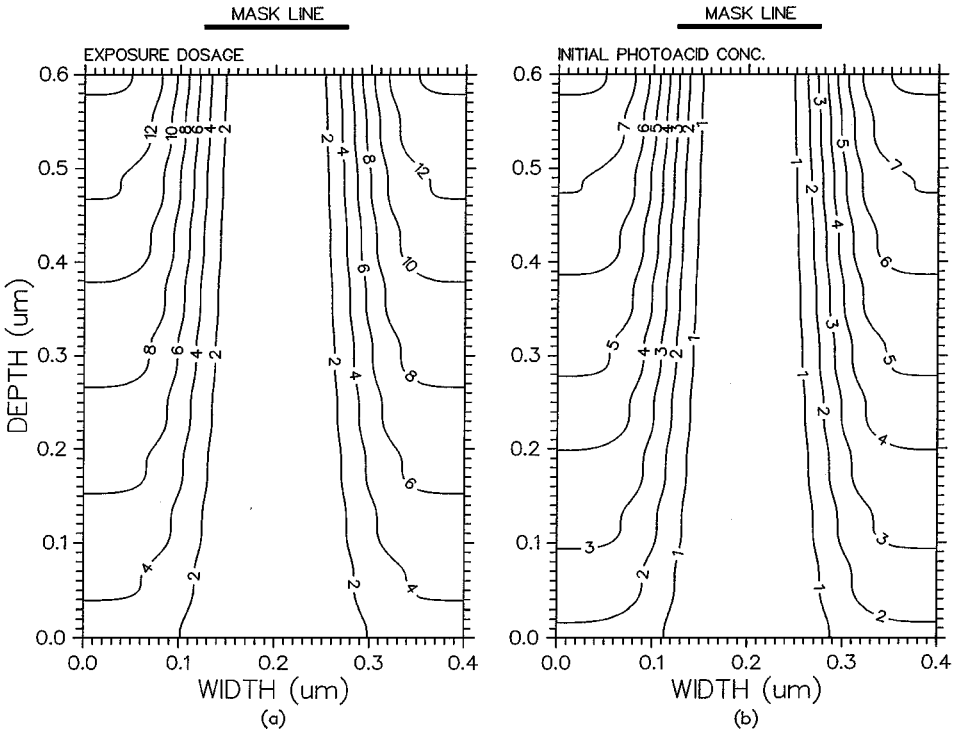


FIG. 2. The exposure dosage (a) and the initial photoacid concentration (b) in units of mJ/cm^2 and $1 \times 10^6/\mu\text{m}^3$, respectively, for the LS pattern.

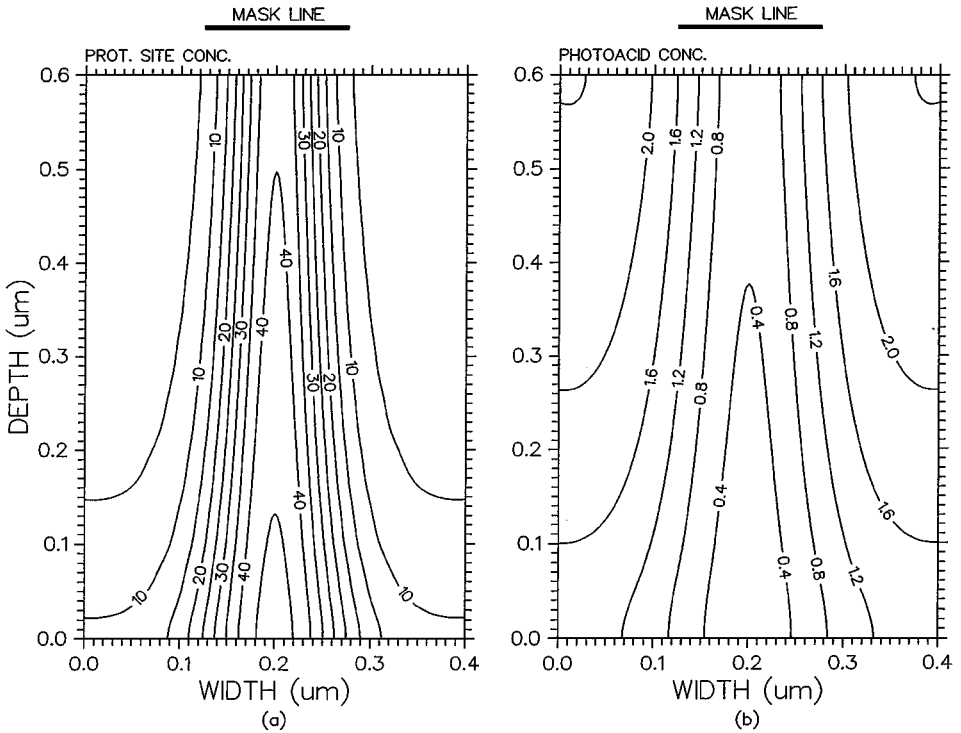


FIG. 3. The protection-site concentration (a) and the acid concentration (b) after the PEB process, for the LS pattern. The room and bake temperatures are taken to be at 23 and 100°C, respectively. The bake time and the total thermal time are taken to be 60 and 120 s, respectively.

0.15 μm long on the top of each LS contour plot represents the mask line. The protection-site and acid concentrations of the LS pattern subject to the baking temperature history of Fig. 1 are, respectively, plotted in Figs. 3a and 3b in units of $1 \times 10^6/\mu\text{m}^3$.

The CH pattern is a contact hole pattern of 0.15 μm and is utilized to exemplify the hole-opening technology of 0.15- μm lithography. The exposure dosage and the initial acid concentration of the CH pattern are given in Figs. 4a and 4b in units of mJ/cm^2 and $1 \times 10^6/\mu\text{m}^3$, respectively. The two heavy line segments on the top of each CH contour plot represent the mask opacity. Hence, the central opening stands for the mask opening. The protection-site and acid concentrations of the CH pattern subject to the baking temperature history of Fig. 1 are, respectively, plotted in Figs. 5a and 5b in units of $1 \times 10^6/\mu\text{m}^3$.

The waviness of the patterns in the postexposure latent image of the LS and the CH structures in Figs. 2 and 4, respectively, is due to the standing-wave effects of the incident beam and is eliminated by the photoacid diffusion as shown in Figs. 3 and 5, respectively.

To concentrate on the effects of the temperature–time history on the PEB process, the resist profiles obtained by the PEB simulations are not passed to a development simulator to obtain the final developed resist profiles [37–38]. Instead, the predevelopment critical dimensions (PDCD) are extracted from the contours of the protection-site concentration. The PDCD is defined to be the length of the continuous interval on the resist/substrate interface with a protection-site concentration of less than $25 \times 10^6/\mu\text{m}^3$. For example, the PDCDs of the LS and CH structures in Figs. 3a and 5a are 0.1499 and 0.1525 μm , respectively.

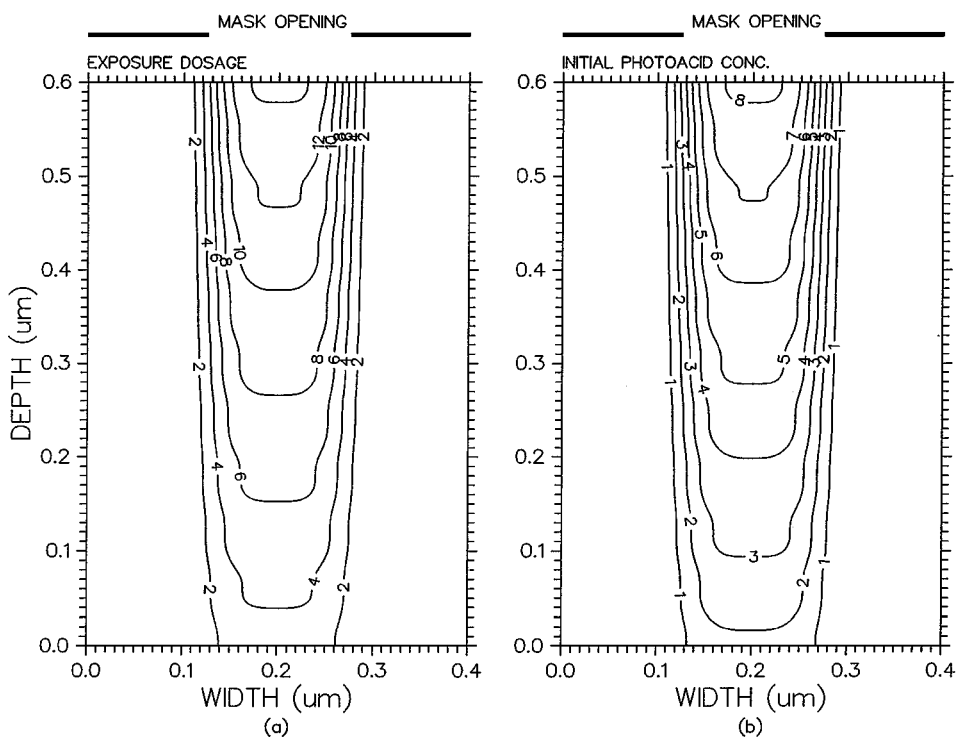


FIG. 4. The exposure dosage (a) and initial photoacid concentration (b) in units of mJ/cm^2 and $1 \times 10^6/\mu\text{m}^3$, respectively, for the CH pattern.

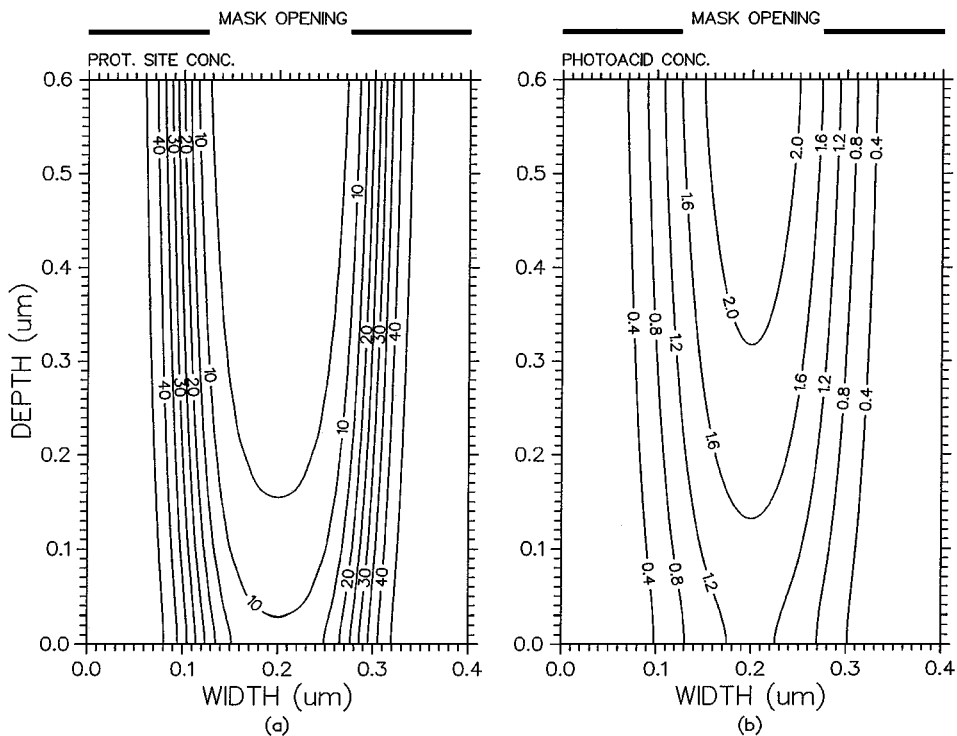


FIG. 5. The protection-site concentration (a) and the acid concentration (b) after the PEB process, for the CH pattern. The room and bake temperatures are taken to be at 23 and 100°C, respectively. The bake time and the total thermal time are taken to be 60 and 120 s, respectively.

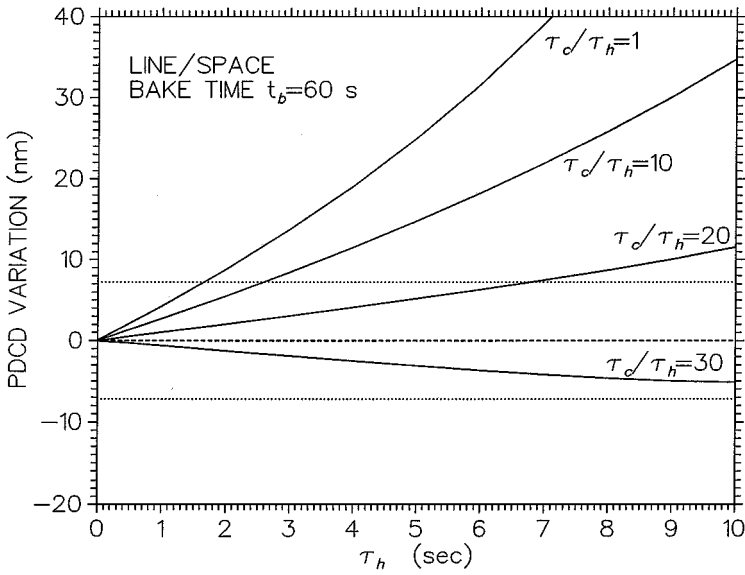


FIG. 6. The PDCD variations of the LS structure are plotted versus the heating time constant for the cooling/heating time constant ratio ($r = \tau_c/\tau_h$) ranging from 1 to 30. The room and bake temperatures are taken to be at 23 and 100°C, respectively. The bake time and the total thermal time are taken to be 60 and 120 s, respectively.

In the above portion of this section, the results of the PEB simulation with a specific combination of modeling parameters are presented in detail. In order to test the simulator for other combinations of parameters, the PDCDs are simulated for different combinations of the heating time constants (τ_h) and the cooling time constants (τ_c) grouped by their ratios, $r = \tau_c/\tau_h$. The ratio is termed the cooling/heating time constant ratio in this work. The condition with $\tau_h = \tau_c = 0$ s corresponds to the case of square-wave heating and cooling and is demonstrated by the dashed lines in Fig. 1, where the baking starts and terminates abruptly.

The PDCD variation is defined to be the signed difference between the PDCD obtained by the PEB process with nonvanishing heating and cooling time constants and the PDCD obtained by the PEB process with square-wave heating and cooling. The PDCD variations for the LS and CH structures are shown in Figs. 6 and 7, respectively, as functions of the heating time constant for various cooling/heating time constant ratios. The horizontal dashed lines in both figures represent $\pm 5\%$ off the PDCDs obtained by the PEB process with square-wave heating and cooling. The PDCDs obtained by the square-wave PEB process are 0.1444 and 0.1577 μm for the LS and CH structures, respectively.

It is found in Figs. 6 and 7 that, at a given heating time constant, the PEB processes with larger heating/cooling time constant ratios ($r = \tau_c/\tau_h$) have smaller PDCD variations. This trend holds for both the LS and CH structures for the heating/cooling time constant ranging from 1 to 30 and can be explained qualitatively as follows.

Since the protection sites are gradually consumed over the course of the bake process, the deprotection reaction gradually slows down as the bake process proceeds. In a sense, the thermal budget is depreciated over the course of the PEB process. In comparison with the square-wave PEB process, the thermal budget deficit in the heating phase of the exponential PEB process has to be compensated by the thermal budget bonus in the cooling phase if the final PDCDs of both PEB processes are to be equal. Given the fact that the thermal

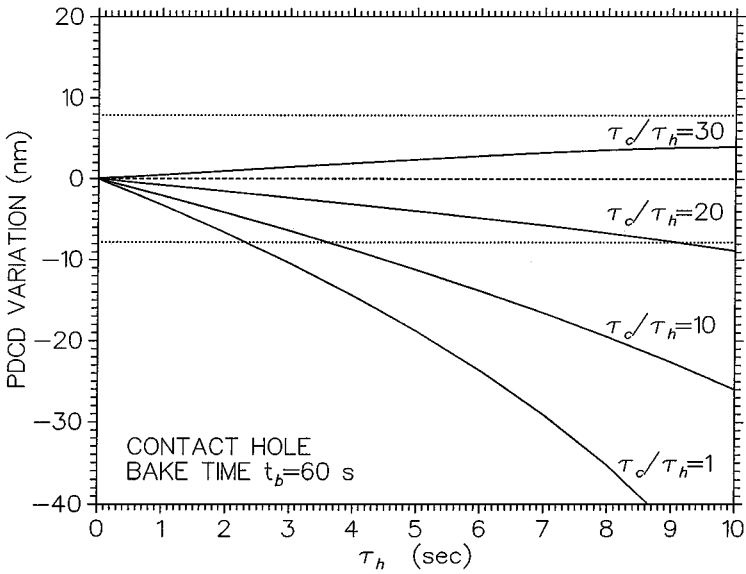


FIG. 7. The PDCD variations of the CH structure are plotted versus the heating time constant for the cooling/heating time constant ratio ($r = \tau_c/\tau_h$) ranging from 1 to 30. The room and bake temperatures are taken to be at 23 and 100°C, respectively. The bake time and the total thermal time are taken to be 60 and 120 s, respectively.

budget is continuously depreciated along the PEB process, the cooling time constant must be larger than the heating time constant to minimize the PDCD variations. Simulations of the square-wave and the exponential PEB processes show that the cooling time constant of the exponential bake process must be 20 to 30 times larger than the heating time constant to have the least variant PDCDs versus the heating time constant [39].

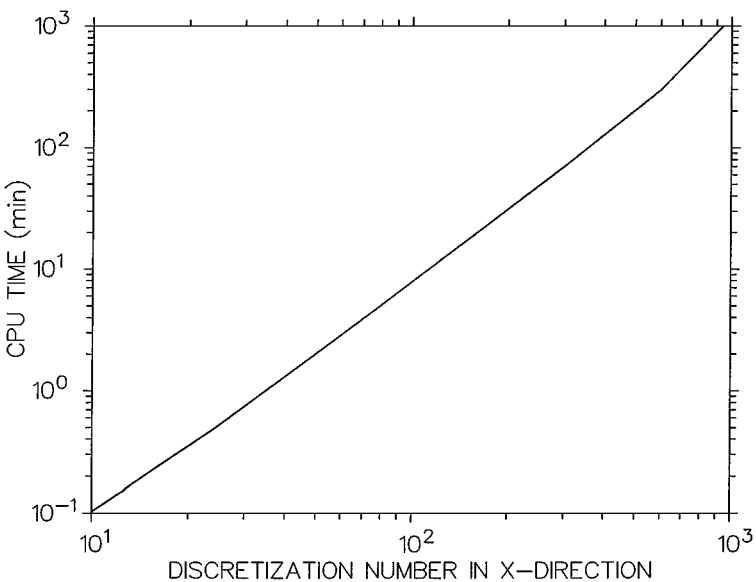


FIG. 8. The CPU time is plotted versus the number of discretizations in the x -direction to illustrate the computational performance of the PEB simulator.

4.3. Computational Performance

The simulation was performed on an AMD Athlon 800-MHz Linux system. The relative error (ϵ) and the absolute error (R) in the time-stepping algorithm given by Eq. (23) are taken to be 10^{-5} and 10^{-8} , respectively. The number of discretizations in the y -direction is 1.5 times that in the x -direction in the plot. Simulations with the rectangular grids ranging from 10×15 to 1000×1500 are performed without any convergence problem. The CPU time versus the number of discretizations in the x -direction is depicted in Fig. 8. For the simulation with 100×150 grids, the required CPU time is less than 8 min. The linearity and slope of the log-log plot in Fig. 8 imply quadratic dependence of the CPU time on the discretization number in one direction, that is, the linear dependence on the total number of grids.

5. CONCLUSIONS

In this article, the PEB process of chemically amplified resists is modeled by a set of reaction-diffusion equations. The model parameters including the reaction parameters and the diffusion coefficients are treated as time-dependent functions in the entire course of the PEB process. With these temperature-dependent model parameters built into the simulator, the heating and cooling stages of the bake process can be simulated.

The alternating-direction implicit method is used to iteratively solve the set of reaction-diffusion equations. An error-control scheme is devised to step the numerical algorithm along the entire baking process. This time-dependent PEB simulator is applied to simulate the resist profiles of line/space patterns and contact holes. It was demonstrated that the algorithm is efficient enough for ordinary hardware to obtain results in reasonable CPU time.

Owing to the time-dependent nature of this PEB simulator, it can be utilized to investigate the effects of temperature-time history of the wafer on the PEB results [40]. The deprotection reaction in the cooling phase is much slower than that in the heating phase because of the continual consumption of protection sites along the bake process. It is found that the cooling/heating time constant ratio between 20 and 30 minimizes the critical-dimension variations between the square-wave and the exponential PEB processes. The PEB simulator developed in this work was proposed to optimize the process window of the PEB process of chemically amplified resists [39].

ACKNOWLEDGMENT

T. L. Li acknowledges the support of the National Science Council, Taiwan through Grant NSC89-2215-E-415-001.

REFERENCES

1. A. A. Lamola, C. R. Szmanda, and J. W. Thackeray, Chemically amplified resists, *Solid State Technol.* Aug. 53 (1991).
2. D. R. McKean, R. D. Allen, P. H. Kasai, U. P. Schaedeli, and S. A. MacDonald, Acid generation and acid diffusion in photoresist films, *SPIE Adv. Resist Technol. Proc. IX* **1672**, 94 (1992).
3. R. A. Ferguson, C. A. Spence, Y. Shacham-Diamand, and A. R. Neureuther, Modeling and simulation of multiple chemical states in photoresist materials, *SPIE Adv. Resist Technol. Proc. VI* **1086**, 262 (1989).

4. J. S. Petersen, C. A. Mack, J. W. Thackeray, R. Sinta, T. H. Fedynyshyn, M. Mori, J. D. Byers, and D. A. Miller, Characterization and modeling of a positive acting chemically amplified resist, *SPIE Adv. Resist Technol. Proc. XII* **2438**, 153 (1995).
5. M. Zuniga and A. R. Neureuther, Postexposure bake characterization and parameter extraction for positive deep-UV resists through broad-area exposure experiments, *SPIE Adv. Resist Technol. Proc. XIII* **2724**, 110 (1996).
6. E.-M. Lee, M.-G. Sung, Y.-M. Lee, Y.-S. Sohn, and H.-K. Oh, Characterization of 193-nm chemically amplified resist during postexposure bake and postexposure delay, *Jpn. J. Appl. Phys.* **38**(12B), 7094 (1999).
7. L. Capodiecì, A. Krasnoperova, F. Cerrina, C. Lyons, C. Spence, and K. Early, Novel postexposure bake simulator: First results, *J. Vac. Sci. Technol. B* **13**(6), 2963 (1995).
8. J. S. Petersen, J. D. Byers, and R. A. Carpio, The formation of acid diffusion wells in acid catalyzed photoresists, *Microelectron. Eng.* **35**, 169 (1997).
9. Y. Yanagishita, S. Miyata, Y. Kaimoto, A. Oikawa, E. Yano, and I. Hanyu, Postexposure-bake simulation model with constant acid loss of chemically amplified resist, *Jpn. J. Appl. Phys.* **36**(12B), 7611 (1997).
10. G. Wallraff, J. Hutchinson, W. Hinsberg, F. Houle, and P. Seidel, Kinetics of thermal and acid-catalyzed deprotection in deep-UV resist materials, *Microelectron. Eng.* **27**, 397 (1995).
11. M. Zuniga and A. R. Neureuther, Reaction–diffusion modeling and simulations in positive deep ultraviolet resists, *J. Vac. Sci. Technol. B* **13**(6), 2957 (1995).
12. E. Croffie, M. Cheng, and A. Neureuther, Moving boundary transport model for acid diffusion in chemically amplified resists, *J. Vac. Sci. Technol. B* **17**(6), 3339 (1999).
13. E. Croffie, M. Cheng, M. Zuniga, and A. Neureuther, Efficient simulation of postexposure bake processes in STORM, *SPIE Adv. Resist Technol. Proc. XVI* **3678**, 1227 (1999).
14. D. E. Bornside, C. W. Macosko, and L. E. Scriven, Spin coating: One-dimensional model, *J. Appl. Phys.* **66**(11), 5185 (1989).
15. D. E. Bornside, C. W. Macosko, and L. E. Scriven, Spin coating of a PMMA/chlorobenzene solution, *J. Electrochem. Soc.* **138**(1), 317 (1991).
16. W. W. Flack, D. S. Soong, A. T. Bell, and D. W. Hess, A mathematical model for spin coating of polymer resists, *J. Appl. Phys.* **56**(4), 1199 (1984).
17. L. M. Peurrung and D. S. Graves, Planarization of spin-coated films, *SPIE Opt./Microlithogr. V* **1674**, 578 (1992).
18. W. J. Lin and W. C. Chen, Theoretical analysis of soft-baking process on a PMMA/anisole solution, in *Proceedings of the Symposium on Nano Device Technology*, 2000, Hsinchu, Taiwan, Lithography Technology and Novel Devices, pp. 154–157.
19. C. A. Mack, D. P. DeWitt, B. K. Tsai, and G. Yetter, Modeling of solvent evaporation effects for hot plate baking of photoresist, *SPIE Adv. Resist Technol. Proc. XI* **2195**, 584 (1994).
20. A. A. Krasnoperova, M. Khan, S. Rhyner, J. W. Taylor, Y. Zhu, and F. Cerrina, Modeling and simulations of a positive chemically amplified photoresist for x-ray lithography, *J. Vac. Sci. Technol. B* **12**(6), 3900 (1994).
21. J. S. Petersen, C. A. Mack, J. Sturtevant, J. D. Byers, and D. A. Miller, Nonconstant diffusion coefficients: Short description of modeling and comparison to experimental results, *SPIE Adv. Resist Technol. Proc. XII* **2438**, 167 (1995).
22. J. W. Thackeray, M. D. Denison, T. H. Fedynyshyn, D. Kang, and R. Sinta, Following the acid: Effect of acid surface depletion on phenolic polymers, *ACS Symp. Ser.* **614**, 110 (1995).
23. L. H. Sperling, *Introduction to Physical Polymer Science*, 2nd ed. (Wiley, New York, 1993).
24. S. L. Rosen, *Fundamental Principles of Polymeric Materials* (Wiley, New York, 1982).
25. F. H. Dill, W. P. Hornberger, P. S. Hauge, and J. M. Shaw, Characterization of positive photoresist, *IEEE Trans. Electron Devices* **22**(7), 445 (1975).
26. N. K. Eib, E. Barouch, U. Hollerbach, and S. A. Orszag, Characterization and simulation of acid catalyzed DUV photoresist, *SPIE Adv. Resist Technol. Proc. X* **1925**, 186 (1993).
27. D. P. DeWitt, T. C. Niemoeller, C. A. Mack, and G. Yetter, Thermal design methodology of hot and chill plates for photolithography, *SPIE Integrated Circuit Metro. Inspect. and Process Control VIII* **2196**, 432 (1994).

28. W. H. Press, S. A. Teukolsky, W. T. Vetterling, and B. P. Flannery, *Numerical Recipes in C, the Art of Scientific Computing*, 2nd ed. (Cambridge Univ. Press, Cambridge, 1992).
29. W. F. Ames, *Numerical Methods for Partial Differential Equations*, 3rd ed. (Academic Press, Boston, 1992).
30. A. Iserles, *A First Course in the Numerical Analysis of Differential Equations* (Cambridge Univ. Press, Cambridge, UK, 1996).
31. H. P. Urbach and D. A. Bernard, Modeling latent-image formation in photolithography, using the Helmholtz equation, *J. Opt. Soc. Am. A* **6**(9), 1343 (1989).
32. D. C. Cole, E. Barouch, U. Hollerbach, and S. A. Orszag, Derivation and simulation of higher numerical aperture aerial images, *Jpn. J. Appl. Phys.* **31**(12B), 4110 (1992).
33. H. Kirchauer and S. Selberherr, Rigorous three-dimensional photoresist exposure and development simulation over nonplanar topography, *IEEE Trans. Comput.-Aided Design* **16**(12), 1431 (1997).
34. A. K. Wong and A. R. Neureuther, Rigorous three-dimensional time-domain finite-difference electromagnetics simulation for photolithographic applications, *IEEE Trans. Semicond. Manuf.* **8**(4), 419 (1995).
35. D. K. Cheng, *Field and Wave Electromagnetics* (Addison-Wesley, Reading, MA, 1983).
36. J. D. Jackson, *Classical Electrodynamics*, 2nd ed. (Wiley, New York, 1975).
37. D. J. Kim, W. G. Oldham, and A. R. Neureuther, Development of positive photoresist, *IEEE Trans. Electron Devices* **31**(12), 1730 (1984).
38. K. K. H. Toh, A. R. Neureuther, and E. W. Scheckler, Algorithms for simulation of three-dimensional etching, *IEEE Trans. Comput.-Aided Design* **13**(5), 616 (1994).
39. T. L. Li and J. H. Ting, Optimal temperature-time condition for the postexposure bake process of deep-UV resists, *Jpn. J. Appl. Phys.* **40**(3B), L259 (2001).
40. C. A. Mack, M. Ercken, and M. Moelants, Matching simulation and experiment for chemically amplified resists, *SPIE Opt. Microlithogr. XII* **3679**, 183 (1999).